Applied Catalysis B: Environmental 232 (2018) 464–471

Contents lists available at ScienceDirect

Applied Catalysis B: Environmental

journal homepage: www.elsevier.com/locate/apcatb

Highly efficient Ni/CeO_2-Al_2O_3 catalysts for CO_2 upgrading via reverse water-gas shift: Effect of selected transition metal promoters

L. Yang[a], L. Pastor-Pérez[a,b,*], S. Gu[a], A. Sepúlveda-Escribano[b], T.R. Reina[a]

[a] Department of Chemical and Process Engineering, University of Surrey, Guildford, GU2 7XH, United Kingdom
[b] Laboratorio de Materiales Avanzados, Departamento de Química Inorgánica Instituto Universitario de Materiales de Alicante Universidad de Alicante, Apartado 99, E-03080 Alicante, Spain

ARTICLE INFO

Keywords:
Reverse water-gas shift
Ni catalyst
Ceria support
Fe promoter

ABSTRACT

In the context of Carbon Capture and Utilisation (CCU), the catalytic reduction of CO_2 to CO via reverse water-gas shift (RWGS) reaction is a desirable route for CO_2 valorisation. Herein, we have developed highly effective Ni-based catalysts for this reaction. Our study reveals that CeO_2-Al_2O_3 is an excellent support for this process helping to achieve high degrees of CO_2 conversions. Interestingly, FeO_x and CrO_x, which are well-known active components for the forward shift reaction, have opposite effects when used as promoters in the RWGS reaction. The use of iron remarkably boosts the activity, selectivity and stability of the Ni-based catalysts, while adding chromium results detrimental to the overall catalytic performance. In fact, the iron-doped material was tested under extreme conditions (in terms of space velocity) displaying fairly good activity/stability results. This indicates that this sort of catalysts could be potentially used to design compact RWGS reactors for flexible CO_2 utilisation units.

1. Introduction

Carbon dioxide (CO_2) is the most widely known greenhouse gas and leads to a range of issues, such as global warming and climate change. More importantly, due to the anthropogenic emissions from conventional fossil fuels consumption, the increase of carbon emissions to the atmosphere is unavoidable. Therefore, the utilisation of CO_2 as a cheap, non-toxic, and huge carbon resource has focused scientist' interests through the production of energy-rich chemicals, being these processes a promising way that may mitigate this global threat [1].

Nowadays, catalytic reduction of CO_2 to CO, known as the reverse water-gas shift (RWGS) reaction (Eq. (1)), is a key intermediate step for many CO_2 hydrogenation processes, such as Sabatier reaction [2,3] and methanol synthesis [4,5]. Nonetheless, the CO_2 consumption by catalytic conversion in 2016 was 207 million tons, being equivalent to 0.5% of the total amount of anthropogenic emissions [6]. In this sense, promoting the utilisation of CO_2 as a carbon feedstock in an efficient and economically viable way for CO_2 valorisation deserves further investigation.

The Fischer-Tropsch (F-T) process has been proposed as a feasible solution for CO_2 conversion, since the H_2/CO ratio (syngas) obtained from the RWGS reaction with an extra input of renewable H_2 is the main raw material for Fischer-Tropsch synthesis, where syngas is converted into valuable fuels [7,8]. As such, it is obvious that using CO_2 rather than fossil fuels as feedstock to produce valuable commodity chemicals is more sustainable and cleaner.

Regarding experimental conditions, the thermodynamics of the RWGS reaction requires high temperatures to reach satisfactory levels of conversion, hence an additional challenge is to improve catalytic activity for the RWGS reaction at lower temperatures maintaining an acceptable CO selectivity [9]. However, the conversion of CO_2 relies on the reversibility of the primary reaction (Eq. (1)) due to thermodynamic equilibrium. Besides, a parallel unwanted reaction, the CO_2 methanation reaction (Eq. (2)), will compete with the RWGS.

$$CO_2 + H_2 \leftrightarrow CO + H_2O \quad \Delta H°298k = +41\ kJ\ mol^{-1} \tag{1}$$

$$CO_2 + 4H_2 \rightarrow CH_4 + 2H_2O \quad \Delta H°298k = -165\ kJ\ mol^{-1} \tag{2}$$

Concerning RWGS catalysts, not only the catalytic activity but also the stability of these materials for the reaction have to be considered. According to previous studies, noble metals such as Rh, Ru, Pt, Re and Pd can be used as active phase [10–12]. But, since noble metals have economic limitations and low natural abundance, continuous efforts should be made in order to find other alternative materials as catalysts. Previous studies reported some activity of Cu and Zn-based catalysts in the RWGS reaction [13–15]. However, these materials presented poor stability for long-term operations at the relatively high temperatures

* Corresponding author at: Department of Chemical and Process Engineering, University of Surrey, Guildford, GU2 7XH, United Kingdom.
E-mail address: l.pastorperez@surrey.ac.uk (L. Pastor-Pérez).

https://doi.org/10.1016/j.apcatb.2018.03.091
Received 12 January 2018; Received in revised form 22 March 2018; Accepted 25 March 2018
Available online 27 March 2018

needed for the process. A study by Chen et al. investigated the reaction mechanism with a Cu/Al_2O_3 catalyst [14]. The study showed that CO_2 dissociation may occur on the surface of metallic Cu to form CO and Cu_2O. Meanwhile, the catalytic activity of Cu was significantly decreased [14]. For a ZnO-based catalyst, its catalytic activity showed significantly decrease with time on stream while running at high temperature. This effect can be attributed to Zn sublimation during the reaction [11]. Recently, Ni has gained the attention of several research teams working in the RWGS due to its relatively high activity and its economic viability compared to the noble metals discussed previously [12]. Additionally, the use of transition metal oxides, such as Al_2O_3, MgO, ZrO_2 and TiO_2, have been investigated as supports for Ni catalysts [11,12,16,17]. Among these metal oxide carriers, researchers have proved that alumina can help the Ni particles dispersion via a large surface area [18]. However, the inherent acidity of Al_2O_3 promotes coking and catalyst sintering during the reaction, what leads to catalyst deactivation. Therefore, during the catalytic process, carbon deposition is easy to occur on the $Ni\text{-}Al_2O_3$ based catalyst [19]. In this scenario, the major challenge is to avoid the deactivation due to carbon deposition on the active surface sites.

To resolve this issue, ceria (CeO_2) has been well studied and shown potentials of better performance. According to Yue et al., ceria can enhance the redox properties of Al-Ce-O supported catalysts when Ni is introduced into CeO_2 lattice [20]. Therefore, a mixed framework of Al_2O_3-CeO_2 with high thermal stability provides a relatively large surface for an optimal active phase dispersion and allows for oxygen vacancies generation on the surface during the catalytic reaction to improve the catalytic performance [21]. Also, the addition of ceria to alumina-based supports decreases the overall acidity thus helping to avoid carbon deposition.

Based on further studies, the addition of a second metal can also be used to promote the active phase. Indeed, bimetallic combinations have proved better performance than their individual components alone [22]. For Ni-Fe materials, it was found that the catalytic activity in the dry reforming of methane increased as compared with monometallic Ni, since a larger Ni dispersion could be achieved [22]. Besides, because of the electronic effect created via metal-metal interactions, the formation of nickel carbide (coke precursor) could be largely avoided, thus leading to less deactivation occurring [23].

From the structural point of view, Cr_2O_3 has been reported to act as an efficient promoter in catalytic formulations for many reactions, such as Fischer–Tropsch synthesis [24], water-gas shift [25], and partial oxidation of methane [26], because Cr_2O_3 can act as a textural promoter to prevent the rapid loss of specific surface area of the support due to thermal sintering under the reaction conditions. Also, it was found that the high oxygen mobility in the crystal lattice of the Cr_2O_3 support, is crucial for inhibiting coke formation on the Ni-based catalysts [27].

After considering the options above, we propose a new family of multicomponent catalysts ($Ni\text{-}Fe_2O_3/CeO_2\text{-}Al_2O_3$ and $Ni\text{-}CrO_3/CeO_2\text{-}Al_2O_3$) for CO_2 valorisation via the reverse water-gas shift reaction. Their catalytic activity and the influence of their physicochemical properties in the exhibited performance is discussed in this study. A fair comparison with reference systems such as Ni/Al_2O_3 and $Ni/CeO_2\text{-}Al_2O_3$ aiming to discern the role of the promoters is also a matter of this work.

2. Experimental

2.1. Catalyst preparation

The cerium-based support was prepared following the wet impregnation method. The necessary amount of $Ce(NO_3)_3{\cdot}6H_2O$ (Sigma-Aldrich) to obtain 20 wt.% CeO_2 was dissolved in ethanol and added to γ-alumina powder (Sasol, SCFa-230). The resulted solution was evaporated under reduced pressure, dried overnight at 80 °C and calcined at 500 °C for 4 h.

The active phases of the catalysts were added by sequential wet impregnation. Firstly, the support was impregnated with Ni $(NO_3)_2{\cdot}6H_2O$ (Sigma-Aldrich) diluted in ethanol, evaporated under reduced pressure in a rotavapor, dried overnight at 80 °C and calcined at 500 °C for 4 h. After that, the solids were impregnated in a similar way with chromium and iron nitrates (Sigma-Aldrich) and then calcined at 800 °C for 4 h respectively. In all samples, the Ni content was calculated to be 10 wt.%. Both Fe and Cr promoted catalysts were prepared to present 5 wt.% of metal oxide. Separately, the same procedure was used to prepare a Ni/Al_2O_3 sample. To summarize, we prepared four catalysts labelled as follow: Ni/Al, Ni/Ce-Al, NiCr/Ce-Al and NiFe/Ce-Al, with equivalent amounts of Ni, CeO_2 and the metal oxide promoters. For the catalytic tests, the samples are sieved and the fraction retained 100–200 μm is selected for the runs.

2.2. Catalyst characterisation

The textural characterization of the catalysts was carried out by N_2 adsorption at −196 °C with an AUTOSORB-6 equipment (QUANTACHROME INSTRUMENTS). Samples were previously outgassed at 250 °C for 4 h.

X-Ray Diffraction (XRD) analysis was undertaken using an X'Pert Pro PANalytical. The diffraction patterns were recorded with Cu K° (40 mA, 45 kV) over a 2 theta range of 5 to 80°, a position sensitive detector using a step size of 0.05° and a step time of 240 s. The powder XRD patterns were further processed using the accompanying software for the equipment, X'PertHighscore Plus°.

The TPR experiments were carried out in a U-shaped quartz cell using a 5% H_2/He gas flowing at 50 mLmin^{-1}, with a heating rate of 10 °C min^{-1}. 50 mg of catalysts were loaded into the quartz reactor that was heated from room temperature to 1000 °C. Hydrogen consumption was followed by on-line mass spectrometry (Pfeiffer, OmniStar GSD 301). Quantitative analysis was done by integration of the reduction signal and comparison with hydrogen consumption of a CuO reference.

The TPO experiments were carried out in the same U-shaped quartz cell using air flowing at 50 mLmin^{-1}, with a heating rate of 10 °C min^{-1}. 50 mg of catalysts were loaded into the quartz reactor that was heated from room temperature to 1000 °C. CO_2 formation was followed by on-line mass spectrometry (Pfeiffer, OmniStar GSD 301).

X-ray photoelectron spectroscopy (XPS, K-ALPHA, Thermo Scientific) was used to analyze the samples' surface. All spectra were collected using Al-K_ radiation (1486.6 eV), monochromatized by a twin crystal monochromator, yielding a focused X-ray spot (elliptical in shape with a major axis length of 400 μm) at 3 mA × 12 kV. The alpha hemispherical analyser was operated in the constant energy mode with survey scan pass energies of 200 eV to measure the whole energy band and 50 eV in a narrow scan to selectively measure the particular elements. XPS depth profiles were obtained by sputtering the specimen with a 1 keV Ar^+ ion beam. XPS data were analysed with Avantage software. A smart background function was used to approximate the experimental backgrounds and surface elemental composition were calculated from background-subtracted peak areas. Charge compensation was achieved with the system flood gun that provides low energy electrons and low energy argon ions from a single source. The samples were reduced ex-situ at 750 °C, and conserved in octane before the analysis.

2.3. Catalytic behaviour

For the catalytic analysis, the catalyst was placed in a U-shape quartz reactor. Before any catalytic measurement, the catalyst was in situ reduced under a hydrogen flow (50 mL min^{-1}) at 750 °C for 1 h. Reaction products were analysed by on-line gas chromatography (coupled with FID and TCD detectors), using a Plot/Q and Molesieve capillary columns to separate the reactants and the products.

For the catalytic tests each catalyst was evaluated within a temperature range of 400–750 °C. The reactants flow was held at a constant weight hourly space velocity (WHSV) of 30,000 mL g^{-1} h^{-1} with a H_2/CO_2 ratio of 4:1. The stability tests were measured at the same space velocity of 30,000 mL g^{-1} h^{-1} with a H_2/CO_2 ratio of 4:1 at 500 °C and 750 °C for 50 h. A final study with harder conditions was carried out in order to force our catalysts for deactivation. First, NiFe/CeAl was tested for 24 hours at a space velocity of 800,000 mL g^{-1} h^{-1} and then the reaction condition was released for another 24 h test at a space velocity of 400,000 mL g^{-} h^{-1}. To have a better comparison, the same study was carried out with Ni/CeAl. The error in CO_2 conversion and CO/CH_4 selectivities for all the experiments is within ± 0.5%, as in previous works using this reaction set-up [28].

The parameters used for measuring the catalytic activity of each sample in this work were CO_2 conversion (Eq. (3)), CO selectivity (Eq. (4)), and CH_4 selectivity (Eq. (5)) [30].

$$CO_2 \text{ conversion } (\%) = ([CO_2]_{In} - [CO_2]_{Out})/([CO_2]_{In}) \times 100 \quad (3)$$

$$CO \text{ selectivity } (\%) = ([CO]_{Out})/([CO_2]_{In} - [CO_2]_{Out}) \times 100 \quad (4)$$

$$CH_4 \text{ selectivity } (\%) = ([CH_4]_{Out})/([CO_2]_{In} - [CO_2]_{Out}) \times 100 \quad (5)$$

3. Results and discussion

3.1. Textural properties

The N_2 adsorption-desorption isotherms are shown in Fig. S1 (see supporting info). All the supports and their corresponding Ni, Ni-Fe and Ni-Cr catalysts exhibit type IV isotherms, typically ascribed to mesoporous materials according to IUPAC classifications. The BET surface area, pore volume, and pore diameter of the supports and calcined catalysts are given in Table 1. The surface areas of the prepared materials ranged from 141–216 m^2 g^{-1} while the primary pore diameters estimated from the maximum in the BJH pore size distribution are around 6.1 nm. The textural properties are governed by the primary γ-alumina support. The expected decrease in surface area and pore volume after metal and oxide introduction is related to partial blockage of pores of the Al_2O_3 support and dilution effect due to the high metal loading. Interestingly, the BET surface is increased upon CrOx incorporation, which coincides with a small increase in the total pore volume. The later matches well with previous studies where chromium was identified as an efficient textural promoter [27].

3.2. XRD

Prior to reactions, the crystalline structure of each fresh (calcined) catalyst was characterised by XRD. Fig. 1 shows the XRD patterns of all calcined catalysts. It can be observed that all catalysts present diffraction peaks at 2θ = 37.6°, 45.8°, 66.8°, attributed to the primary support γ-Al_2O_3 (JCPDS 00-048-0367).

Regarding ceria containing samples (NiFe/CeAl, NiCr/CeAl and Ni/CeAl), each of the diffraction patterns shows the specific peaks related to the CeO_2-based support used in the corresponding formulation. Peaks appearing at 2θ = 28°, 33.2°, 47.7° and 56.6° indicate the presence of

Table 1
Textural properties of supports and catalysts.

Samples	BET (m^2/g)	Total Pore Volume (cm^3/g)	Pore Size (nm)
Al_2O_3	216	0.513	6.15
20% Ce-Al	159	0.361	6.14
NiAl	187	0.432	6.16
Ni/CeAl	141	0.308	6.14
NiFe/CeAl	146	0.302	6.09
NiCr/CeAl	161	0.275	6.15

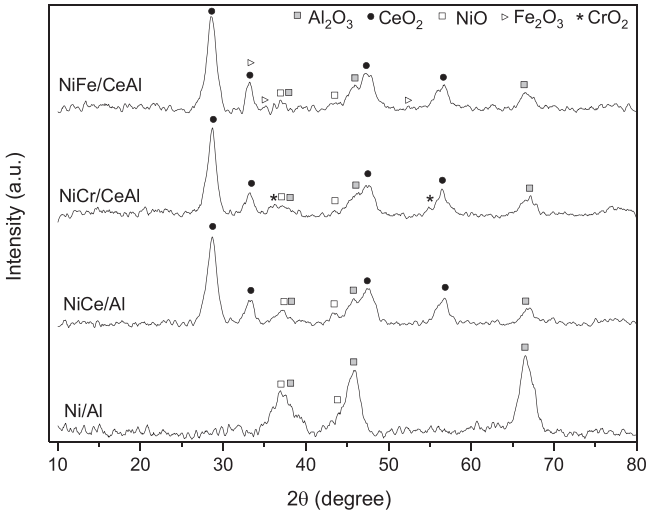

Fig. 1. X-ray diffraction patterns of calcined samples.

fluorite-type CeO_2 cubic crystal structure (JCPDS 34-0394) [30]. Fig. 1 also shows the characteristic NiO peaks (JCPDS 04-0835) at 37.2°, and 43.2°, corresponding to the (111), and (200) planes of the NiO fcc phase [31]. The diffraction peaks of NiO are broad and with low intensity, what reveals that NiO crystallites are small and well dispersed over the support surface. Indeed, it is well-known that the presence of CeO_2 favours the dispersion of NiO [32]. Due to the overlap of the diffraction peaks, the formation of the $NiAl_2O_4$ spinel phase cannot be fully discarded.

For the Cr and Fe doped samples we have labelled the typical positions for the expected reflections of the oxides on Fig. 1. However, it is too difficult to confirm the presence of these oxides by XRD due to the low amount of these promoters in the samples and to the fact that these small peaks can be due to background noise.

3.3. Reducibility: H_2-TPR

The redox properties of the catalysts and the interactions between the metals and the support can be assessed by H_2-TPR studies. Furthermore, this technique can help to elucidate the influence of the promoter on the reducibility of a specific compound in a multi-component system. In Fig. 2, the type of reducible species for each of the samples formed at a certain temperature can be observed. The TPR

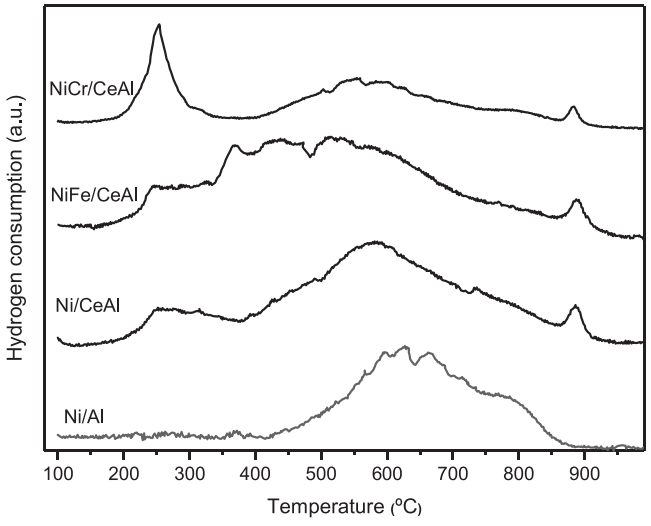

Fig. 2. H_2-TPR profiles of the prepared catalysts.

profiles of all samples show a broad reduction peak at around 600 °C that can be attributed to the reduction of Ni oxide with strong interaction with the Alumina support [33]. Furthermore, it could also be assigned to the reduction of $NiAl_2O_4$ spinel, which is hardly detected by XRD [29].

For the Ce-containing catalyst, the addition of CeO_2 gives a broad reduction peak around 250 °C due to the Ni-Ce interaction. As previously reported elsewhere, the presence of ceria improves Ni reducibility at lower temperatures and the overall redox properties of all the studied catalysts due to its excellent oxygen mobility [34]. Furthermore, a distinctive peak at a higher temperature (875 °C) can be observed on the profiles of Ni/CeAl, NiCr/CeAl and NiFe/CeAl, which is associated to the reduction of bulk ceria [34].

As can be seen clearly in the Cr and Fe doped catalysts, the addition of the second component can strongly influence the reducibility of monometallic Ni-based catalysts [35]. As for the NiCr/CeAl catalyst, one sharp reduction zone at temperatures around 250 °C can be observed, corresponding to the reduction of Cr^{6+} to Cr^{3+} [36]. Moreover, this peak can be also attributed to the simultaneous reduction of a part of Ni oxide species interacting with chromium [37].

In the case of NiFe/CeAl, apart from the first and the final reduction peaks associated with the interaction between Ni-CeO_2 and Ni-Al_2O_3 respectively, there is a broad band which can be observed at intermediate temperatures range overlapping with the first peak. This broad band at a medium temperature is ascribed to the reduction of Ni oxide and dispersed Fe (III) and Fe (II) specis with different interactions. It can be pointed out that addition of Fe slightly shifts the reduction of Ni oxide interacting with Al_2O_3 to lower temperatures. In this case, also the presence of Fe oxide (and the formation of more oxygen vacancies) improves the reduction of NiO [38].

In order to have a quantitative estimation of the reducibility of the studied samples, the reduction percentage (RP) of every system has been calculated according to the equation below [39]:

$$RP(\%) = \frac{E_{HC}}{T_{HC}} * 100$$

In this equation, T_{HC} is the theoretical hydrogen consumption (in moles) required for the complete reduction of all the reducible cations present in the solid and E_{HC} is the experimental total hydrogen consumption measured during the TPR. For the calculation of T_{HC}, we have considered that all cations are initially in their maximum oxidation state, (Ni^{2+}, Ce^{4+}, Fe^{3+}, Cr^{6+}).

As shown in Fig. 3 the addition of ceria, iron oxide and chromium oxide increases the reducibility of the un-promoted Ni/Al catalyst. In fact, all the doped catalysts presented an RP over 90% while the reference Ni/Al catalyst showed an RP of 86.5%. The observed effect is mainly related to two factors happening simultaneously: (i) the promoters weaken the Ni-Al_2O_3 interaction enhancing Ni particles reducibility due to the created Ni-promoter contact (ii) all the selected promoters CeO_2, FeOx and CrOx provide extra oxygen mobility to the catalysts due to their inherent redox properties. The latter is a relevant property for redox reactions such as the RWGS and therefore may have an effect on the catalytic behaviour. It should be highlighted that the Fe doped catalyst is the system with the highest reducibility within studied series and also it is the one with the most homogenous reducibility profile as evidenced in Fig. 3.

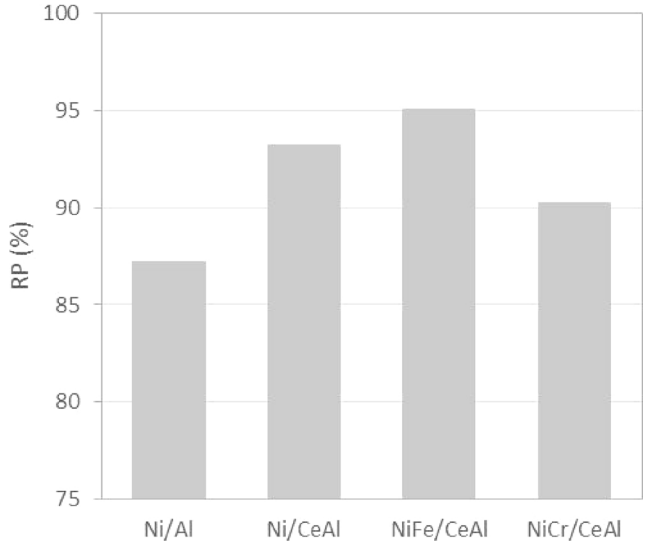

Fig. 3. Reduction percentage (RP) of the prepared solids.

3.4. XPS characterization of reduced catalysts

In contrast, while XRD is a bulk technique, XPS is able to measure elements from the topmost layers of 3–5 nm thick slabs of the surface species, what is essential to discern the chemical status of the catalytic active species.

The Ni $2p_{3/2}$ spectrum of all reduced samples can be observed in Fig. 4(a), and Table 2 summarizes the main peaks of the Ni $2p_{3/2}$, Fe $2p_{3/2}$ and Cr 2p energy levels. In order to reproduce as far as possible the catalysts status before the reaction runs, the samples were pre-reduced 750 °C before the XPS analysis. As can be seen in Fig. 4, after the reduction only a part of Ni was in the metallic state and different nickel species co-exist in the reduced catalysts as can be seen in the complex Ni $2p_{3/2}$ spectra. In this way, for all catalysts the band around 851–853 eV is assigned to Ni°; the following two bands, at around 854 and 857 eV are ascribed to two types of surface Ni^{2+} due to the different interactions with Al_2O_3 and/or CeO_2 [40].

Additionally, as shown in Table 2, the Ni B.E. of the $2p_{3/2}$ level in the reduced Ni/Al catalyst (853.16 eV) appears at higher values compared to the Ce-containing and Cr, Fe promoted samples. This indicates the existence of a strong metal-support interaction between Ni and Al_2O_3 that can modify the structure and electronic properties of Ni, avoiding its reduction [41]. Furthermore, this higher value is in agreement with the H_2-TPR results, which leads to a lower Ni reducibility in this sample.

Bonnelle et al. [42] proposed that nickel aluminate is characterised by a Ni $2p_{3/2}$ binding energy of 855.8 eV. The Ni $2p_{3/2}$ spectrum for the Ni/Al sample exhibits a peak at 855.24 eV that is at slightly higher BE than that of bulk NiO (855.1 eV) and may contain contributions from $NiAl_2O_4$-like species present on the surface as suggested in TPR and XRD discussion. In contrast, for the Ce-containing samples, this value is lower for all of them since CeO_2, due to its excellent redox properties, enhances the Ni reducibility in these catalysts, a fact that is also in agreement with the H_2-TPR results.

For the Fe- and Cr-doped samples, it should be pointed out that a notorious shift to lower Ni B.E. values was obtained for these samples, what indicates that Fe and Cr appear to hinder the strong interaction between nickel and alumina, thus favouring metallic nickel formation [43]. This fact is more notorious for the NiFe/CeAl catalyst, in which the nickel electronic environment is probably altered by iron, which results in an electronic enrichment as reflected in the observed B.E. value for the Ni photoelectron at 851.3 eV [9]. This indicates that in the Fe-doped materials, Ni is electronically richer than in the rest of the samples, a fact that could affect the catalytic performance.

Fig. 4(b) shows the Fe $2p_{3/2}$ core level XPS spectrum of the NiFe/CeAl catalyst. According to previous results in the literature, the band at 711.1 eV corresponds to the Fe^{3+} oxidation state, the band at 709.9 eV can be attributed to the Fe^{2+} and the band at lower binding energies, 705.5 eV, corresponds to metallic Fe [44]. Therefore, despite the reduction treatment at 750 °C, a combination of Fe species coexist in this sample. Finally, Fig. 4(c) illustrates the Cr 2p XPS spectra of the Cr promoted sample. The peak at 577.7 eV is typically characteristics of Cr^{3+} species [29] that means that all Cr was reduced from Cr^{+6} to Cr^{+3}

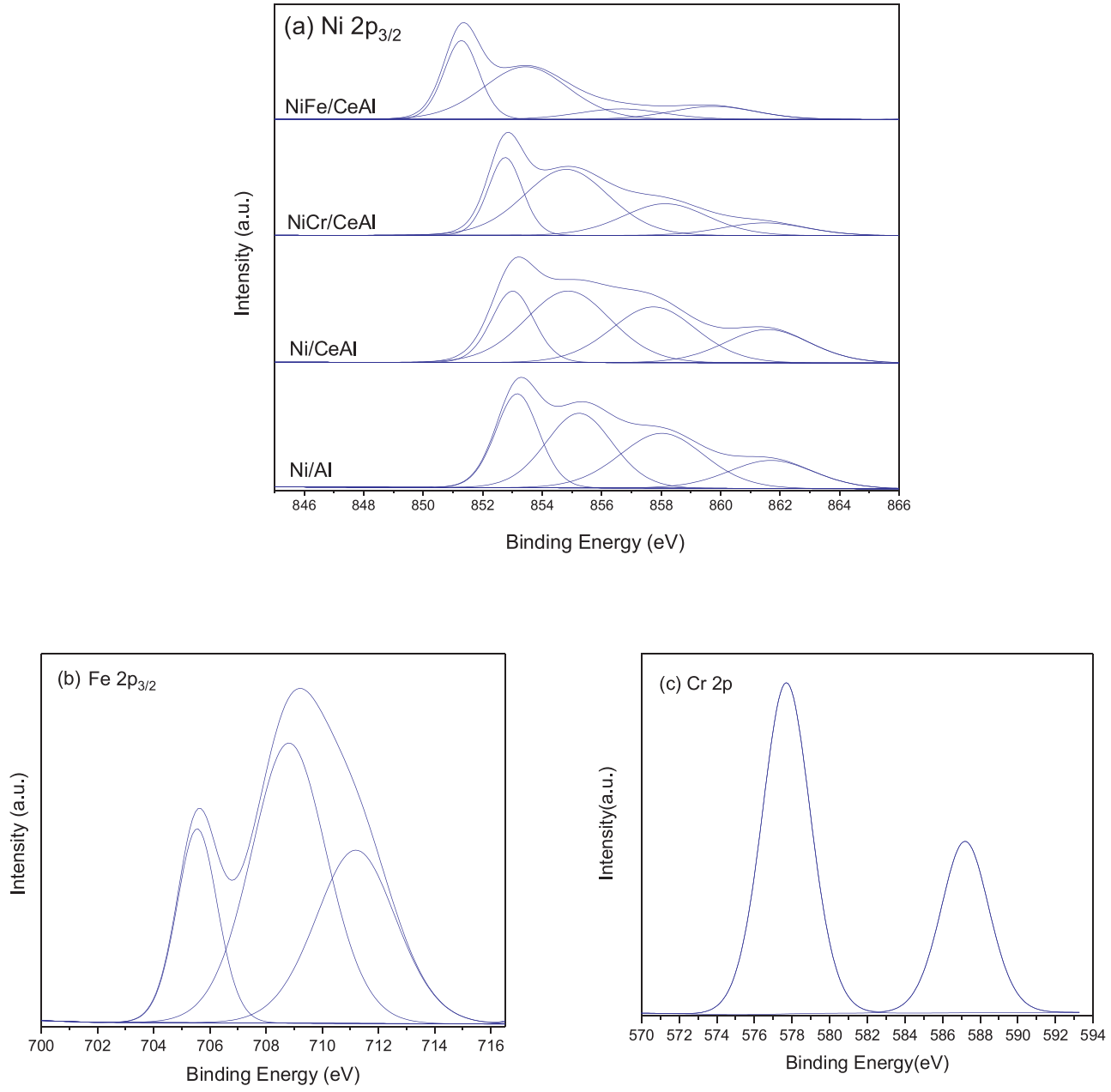

Fig. 4. XPS spectra of (a) Ni $2p_{3/2}$ region for all samples, (b) Fe $2p_{3/2}$ region for the NiFe/CeAl catalyst and (c) Cr 2p region for the NiCr/CeAl catalyst.

Table 2
Binding energies of the Ni $2p_{3/2}$, Fe $2p_{3/2}$ and Cr 2p levels for the reduced catalysts and Ni/Al and Ce/Al atomic ratios.

Catalysts	Ni $2p_{3/2}$ (eV)		Fe $2p_{3/2}$ (eV)			Cr 2p (eV)	Ni/Al (at./at.)	Ce/Al (at./at.)
	Ni^{2+}	Ni°	Fe^{3+}	Fe^{2+}	Fe	Cr^{3+}		
NiFe/CeAl	853.44 856.66	851.29	711.19	708.81	705.55	–	0.221	0.061
NiCr/CeAl	854.81 858.14	852.76	–	–	–	577.70	0.034	0.076
NiCe/Al	854.87 857.75	853.01	–	–	–	–	0.024	0.038
Ni/Al	855.24 858.02	853.16	–	–	–	–	0.022	–

as suggested in the TPR section.

Ni and Ce atoms dispersions on the catalysts' surface were estimated using Ni/Al and Ce/Al ratios as reported in Table 2. As shown in the table, Ni/Al ratio increases upon addition of promoters. In particular, the Fe-doped sample presents a remarkable high value for Ni/Al which indicates a strong enrichment of Ni atoms on the catalyst's surface. Therefore, we can clearly state that Fe addition boosts Ni dispersion as we intended with this promoter and in good agreement with previous results in literature for dry reforming using Ni-Fe catalysts [22]. Similarly, the Ce/Al ratio is higher (almost double) for Cr and Fe doped catalysts in comparison with the non-promoted Ni/CeAl sample evidencing the benefits for ceria dispersion.

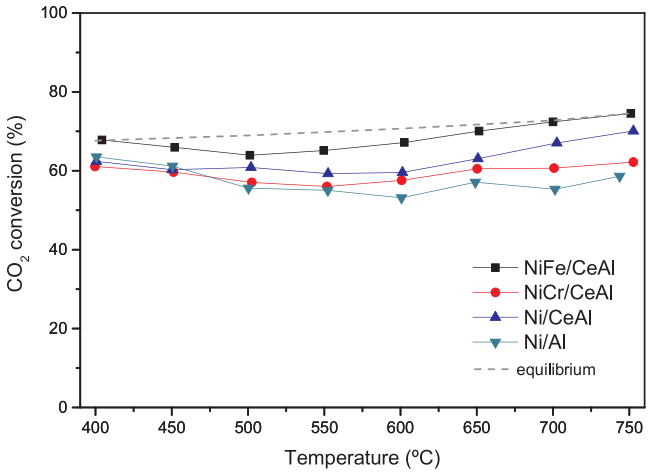

Fig. 5. CO_2 conversion for all catalysts as a function of temperature.

3.5. Catalysts performance

3.5.1. Catalytic activity, selectivity and post reaction characterisation

After understanding the surface and redox chemistry of our materials, we tested all the synthesized catalysts in the RWGS reaction to study their catalytic performance. In Fig. 5, the catalytic behaviour of all samples, in terms of CO_2 conversion as a function of temperature, is reported. It can be seen the superior activity of the Ni/CeAl and NiFe/CeAl catalysts over the Ni/Al and the NiCr/CeAl catalysts. Indeed, these two catalysts reached CO_2 conversion levels rather close to the thermodynamic equilibrium, being the Fe-promoted sample the best material within the studied series. The excellent behaviour of the Fe-doped sample could be ascribed to the electronic state of Ni in this sample. Indeed, as discussed in the XPS section, Ni in this material is electronically richer due to the presence of iron as redox promoter and the close Ni-FeO_x interaction. Such interaction results in the electronic transfer from to FeO_x to Ni that increases the electronic density of Ni atoms and makes them more reactive and ready to overcome the CO_2 activation.

It has to be pointed out the high CO_2 conversion reached with this series of catalysts at lower temperatures. The presence of Ni favours the catalytic behaviour at lower temperatures compared to other metals [28], but not always in favour of the desired reaction. The activity enhancement at low temperatures would greatly favour heat integration with a potential Fischer-Tropsch unit if it is accompanied with a good CO selectivity [28].

In this sense, the selectivity profiles (Fig. 6) clearly mirror the competition RWGS/CO_2 methanation reaction. For all the studied samples the selectivity to methane decreases with temperature while the CO selectivity shows the opposite trend (i.e. CO selectivity increases with temperature). Briefly, it seems that the methanation reaction is favoured in the low-temperature range (400–600 °C) while the reverse water-gas shift becomes dominant as off 600 °C. Surprisingly, the Cr-doped material presented the poorest selectivity towards CO at all studies temperatures. In principle, it could be expected that the presence of CrO_x as dopant should boost the RWGS given the fact that CrO_x is a well-known material for the forward WGS. Nevertheless, it seems that CrO_x may help Ni for the secondary reaction (CO_2 methanation) especially at high temperatures, where this parallel process is less favoured. Ni/Al shows an intermediate behaviour, displaying better selectivity towards CO than the Cr-doped sample but lower than the NiFe/CeAl and the Ni/CeAl catalysts. The latter confirms the impact of ceria in the catalytic activity and selectivity of the multi-component materials, indicating the suitability of this redox promoter for the RWGS. As for the NiFe/CeAl and the Ni/CeAl, despite the former is more active than the later, the differences in selectivity are minimal

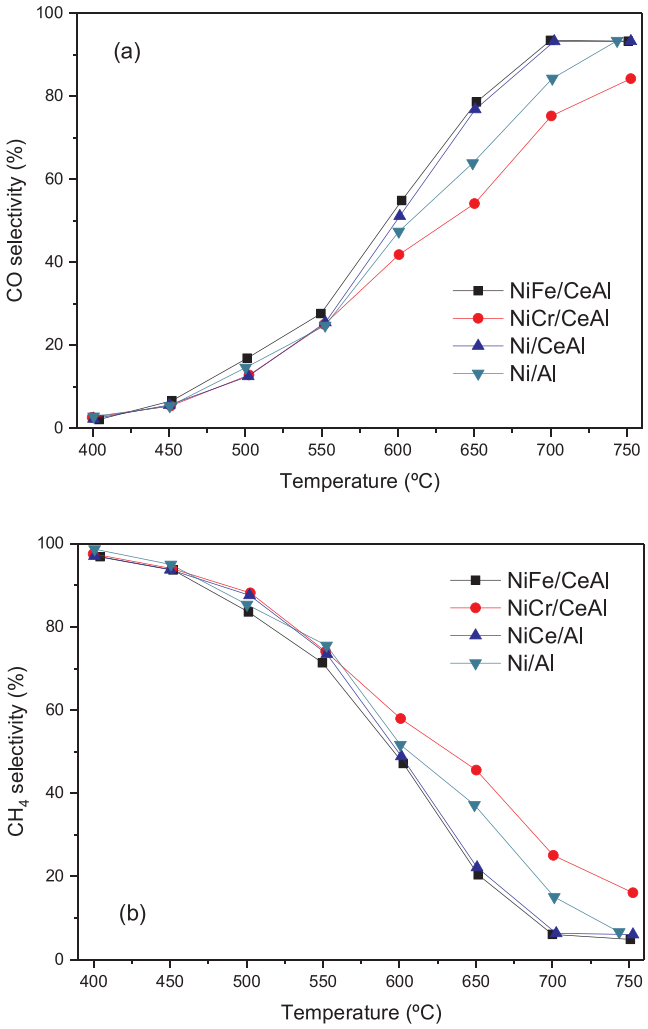

Fig. 6. a) CO selectivity and b) CH_4 selectivity for all catalysts as a function of temperature.

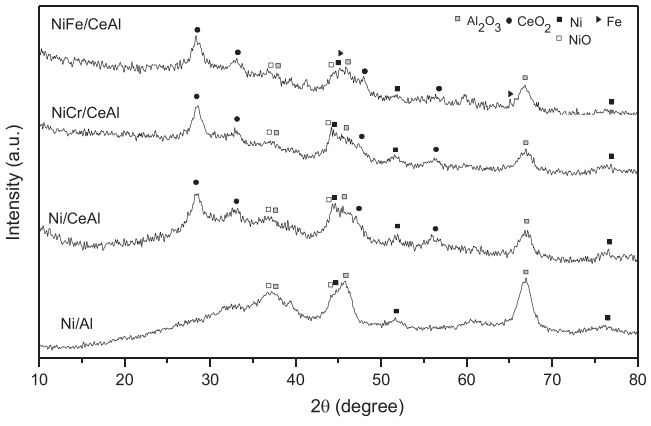

Fig. 7. X-ray diffraction patterns of spend catalysts (400–750 °C, 30,000 mL g^{-1} h^{-1}, H_2/CO_2 ratio of 4:1).

thus making a necessary further investigation to elucidate the discrepancies between these systems.

Post reaction XRD (Fig. 7) shows that all the studied catalysts are rather robust since no sintering of the active phases nor peaks attributed to crystalline carbon species were observed. It is worth mentioning that the spent catalysts present the typical diffraction lines for metallic Ni at 2θ = 44.4°, 51.7°, 76.8° (JCPDS no. 04-0850). In fact, as discussed

in the XPS section, metallic Ni is the main active phase for this reaction whose electronic environment has been altered by the presence of the promoters. The main diffraction peaks for metallic Fe 2θ = 44.7°, 65.0° (JCPDS no. 06-0696) are intended, however, this is a complex zone of the XRD profile where Al_2O_3, Ni and Fe appear.

Aiming further details for carbon deposition a post-reaction TPO study was performed. As depicted in Fig. S2 (see supporting information) all the samples presented small amounts of carbon deposits on the surface after the RWGS. However, these carbonaceous species are soft-like carbon since they can be removed from the catalysts surface at low temperatures (below 400 °C). The later corroborates the tolerance of our multicomponent catalysts towards carbon poisoning and sintering for short-term runs.

3.5.2. Stability study and post reaction characterisation

From Figs. 5 and 6 it is clear that NiFe/CeAl and Ni/CeAl exhibit the best activity/CO selectivity balance in the whole range of studied temperatures, being even better at temperatures above 600 °C. In fact, their excellent behaviour at temperatures above 600 °C is a remarkable matter given the fact that deactivation phenomena such as sintering and coking normally take place at this temperature range [45,46]. Thus, the stability of these two catalysts was tested for 48 h at 750 °C and 500 °C at the same conditions (WHSV of 30,000 mL g^{-1} h^{-1} with a H_2/CO_2 ratio of 4:1) aiming to find further discrepancies between these materials. Results are reported in Fig. 8.

At conditions close to equilibrium (750 °C) the graph shows that CO_2 conversion remains approximately constant at 65% and 70% for Ni/CeAl and NiFe/CeAl, respectively, over the 48 h time period. However, when the samples are studied far from equilibrium (500 °C) the Fe doped sample maintains its high activity and stability while the Ni/CeAl sample suffers for a slight deactivation. In fact, for this catalyst, the conversion dropped from 58% to 50% after 48 hours of continuous operation. Fig. S3 shows the post-stability (at 750 °C) XRD profiles of both Ni/CeAl and NiFe/CeAl samples revealing that Ni sintering starts to be notable in comparison to that observed for short runs. Also in the case of the iron doped catalysts, iron sintering could contribute to the shaper shape of the Ni peak. In both cases, carbon crystalline species were not detected indicating that carbon deposition is irrelevant under these reaction conditions. Overall, these stability tests indicate great stability for long runs with a CO selectivity over 98% in good agreement with the catalytic screening experiments presented in Figs. 5 and 6.

Despite the best catalytic behaviour for the Fe-doped sample in terms of CO_2 conversion, this difference with the NiCe/Al sample was not enough significant to stand out NiFe/CeAl as a better catalyst. For comparison, another stability test under harder conditions was carried

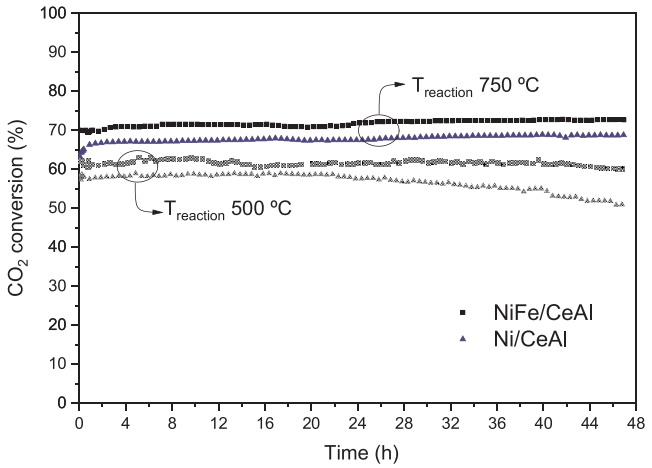

Fig. 8. Stability test at 750 °C and 500 °C, WHSV of 30,000 mL g^{-1} h^{-1} with a H_2/CO_2 ratio of 4:1 for NiFe/CeAl and Ni/CeAl.

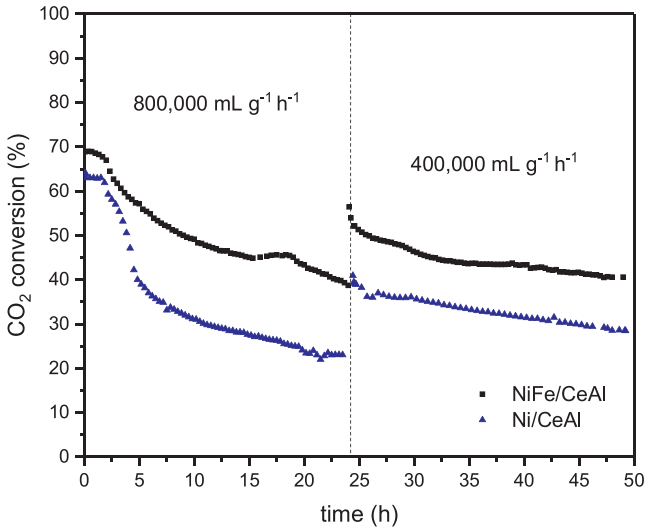

Fig. 9. CO_2 conversion for NiFe/CeAl and NiCe/Al samples at hard conditions.

out to force our catalysts away from thermodynamic equilibrium and also to contribute to facilitating Ni particles sintering. Fig. 9 shows the CO_2 conversion for NiFe/CeAl and NiCe/Al samples at different conditions: a space velocity of 800,000 mL g^{-1} h^{-1} for the first 24 h and then the space velocity was released to 400,000 mL g^{-1} h^{-1} for the next 24 h, both periods with a H_2/CO_2 ratio of 4:1 and a constant temperature of 750 °C. It must be highlighted that these operating conditions are extreme in terms of space velocity and were used to force deactivation.

From Fig. 9, it can be seen that there is an obvious decrease in CO_2 conversion during the first 24 h test at a space velocity of 800,000 mL g^{-1} h^{-1} for both samples. Such a deactivation phenomenon is more prominent for the Ni/CeAl sample, whose activity drops from 64% to 23% in 24 h while the Fe-doped catalyst drops from 70% to 40%. When the space velocity is released to 400,000 mL g^{-1} h^{-1} for the immediate 24 h test, the CO_2 conversion was almost restored for the NiFe/CeAl (± 10% of conversion) and improved but not recovered at all for the Ni/CeAl. In both cases, the conversion drops again with reaction time, but overall, NiFe/CeAl exhibits a better catalytic activity and stability than the Ni/CeAl even under extreme conditions. Since Fe-promoted catalyst is the best catalyst of this study, a detailed post reaction XRD analysis was performed for this sample to get further insights on how the different reaction conditions affect its structure. As shown in Fig. 10, the pre-reduced and the spent samples after the catalytic screening presents a very similar XRD pattern evidencing almost no changes during these tests. For the stability study at 700 °C, Ni particles start to sinter but no carbon deposition or FeOx segregation is observed. Finally, for the stability tests at hard conditions (very high space velocities) crystalline carbon deposits start to nucleate and Ni sintering is more pronounced. Interestingly, sintering of metallic iron is not clearly observed (it might happen but the peaks could overlap with other species of the multicomponent catalyst) and signals of Fe_2O_3 appeared. As discussed in the XPS section part, the Fe species remain partially oxidized on the catalysts' surface after the reduction treatment but they are no appreciable on the XRD. After the stability tests at hard conditions, these particles could have sintered and also extra Fe_2O_3 could have been formed due to oxidization of metallic iron in the presence of high amounts of water as a reaction product. These factors account for the observed deactivation under these demanding conditions which are clearly over specified to force the breakdown.

Overall, the outstanding performance exhibited by the Fe-promoted catalyst under vast space velocities regimes must be underlined from the engineering perspective. Having in mind the application of these materials in a CO_2 conversion unit (i.e. in a typical cement or steel

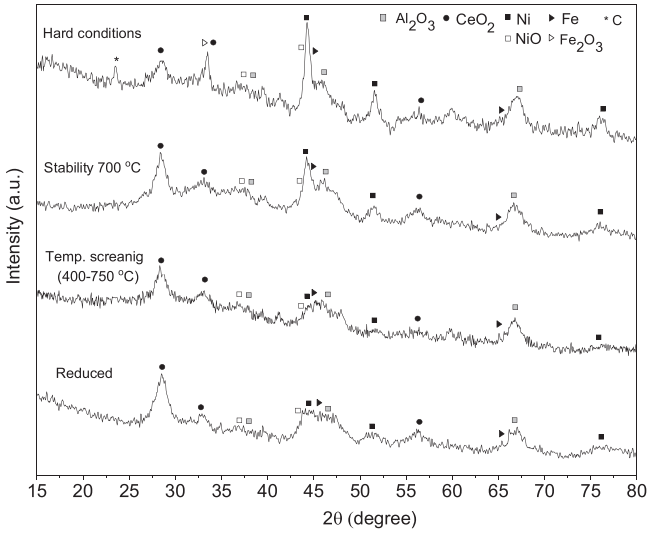

Fig. 10. X-ray diffraction patterns of NiFe/CeAl catalyst at different conditions.

plant) stable performance at such high space velocities would result in a compact reactor design (typically the volume of the reactor has an inverse relation with the space velocity) and, therefore, this could significantly reduce the capital cost investment.

4. Conclusions

The conversion of CO_2 into CO (and syngas) is viable via the RWGS reaction using Ni-based materials. This study reveals that a reference catalyst such as Ni/Al_2O_3 can be highly promoted by the addition of different components such as CeO_2 and FeO_x. In particular, the multicomponent material based on $Ni\text{-}FeO_x/CeO_2\text{-}Al_2O_3$ is an excellent catalyst for the RWGS reaction, leading to high levels of CO_2 conversion and exceptional stability. The outstanding activity/selectivity balance reached by this catalysts is attributed to an electronic enrichment of the Ni surface atoms due to the FeO_x-Ni interaction. Very likely, the higher electronic density of this material facilitates CO_2 adsorption, which is the rate-limiting step. In addition, FeOx greatly enhances Ni dispersion on the surface which also helps to deliver higher activity in the reactions. On the contrary, the use of CrO_x as promoter does not help in the reverse water-gas shift reaction and in turn, it favours the competitive process (CO_2 methanation). In any case, CrOx slightly improves the textural properties and the dispersion of Ni and ceria in the developed catalyst.

Interestingly, our multicomponent catalyst promoted with iron can perform at extreme space velocities showing good catalytic behaviour. The later would facilitate the utilisation of this catalyst to design compact CO_2 conversion units for flexible applications in flue gas processing.

Acknowledgement

Financial support for this work was provided by the Department of Chemical and Process Engineering at the University of Surrey and the EPSRC projects EP/J020184/2 and EP/R512904/1 as well as the Royal Society Research Grant RSGR1180353. The Spanish team acknowledges Ministerio de Economia, Industria y Competitividad of Spain (Project MAT2013-45008-P). LPP also thanks Comunitat Valenciana for her postdoctoral fellow (APOSTD2017).

Appendix A. Supplementary data

Supplementary material related to this article can be found, in the online version, at doi:https://doi.org/10.1016/j.apcatb.2018.03.091.

References

[1] X. Sun, X.L. Yang, B. Zhao, J. Energy Chem. 000 (2017) 1–14.
[2] J. Xu, X. Su, H. Duan, B. Hou, Q. Lin, X. Liu, X. Pan, G. Pei, H. Geng, Y. Huang, T. Zhang, J. Catal. 333 (2016) 227–237.
[3] Z.G. Fan, K.H. Sun, N. Rui, B.R. Zhao, C.J. Liu, J. Energy Chem. 24 (2015) 655–659.
[4] X.D. Xu, J.A. Moujin, Energy Fuels 10 (2) (1996) 305–325.
[5] M. Huš, V.D.B.C. Dasireddy, N.S. Štefanic ̆ c ̆, B. Likozar, Appl. Catal: B. 207 (2017) 267–278.
[6] A. Shima, M. Sakurai, Y. Sone, M. Ohnishi, T. Abe, San Diego, California, 15–19 July 2012, Forty-Second International Conference on Environmental Systems, AIAA (2012) 3552.
[7] G. Centi, E.A. Quadrelli, S. Perathoner, Energy Environ. Sci. 6 (2013) 1711–1731.
[8] D.H. Kim, S.W. Han, H.S. Yoon, Y.D. Kim, Ind. Eng. Chem. 23 (2015) 67–71.
[9] P.M. Maitlis, A. Klerk, Greener Fischer-Tropsch Processes for Fuels and Feedstocks, John Wiley and Sons, 2013.
[10] L. Lloyd, D.E. Ridler, M.V. Twiggin, The Water Gas Shift Reaction, Catalyst Handbook, 2nd ed, Mansion Publishing House, London, 1996, pp. 283–338.
[11] F.M. Sun, C.F. Yan, Z.D. Wang, C.Q. Guo, Int. J. Hydrog. Energy 40 (2015) 15985–15993.
[12] L.H. Wang, H. Liu, Y. Liu, Y. Chen, S.Q. Yang, Rare Earth 31 (2013) 559–564.
[13] M.J. Gines, A.J. Marchi, C.R. Apesteguia, Appl. Catal. A: Gen. 154 (1997) 155–171.
[14] C.-S. Chen, W.H. Cheng, S.-S. Lin, Catal. Lett. 8 (2000) 45–48.
[15] S.W. Park, O.S. Joo, K.D. Jung, H. Kim, S.H. Han, Appl. Catal. A: Gen. 211 (2001) 81–90.
[16] S. Damyanova, B. Pawelec, K. Arishtirova, J.L.G. Fierro, Int. J. Hydrog. Energy 37 (2012) 15966–15975.
[17] S. Aghamohammadi, M. Haghighi, M. Maleki, N. Rahemi, Mol. Catal. 431 (2017) 39–48.
[18] D. Pakhare, J. Spivey, Chem. Soc. Rev. 43 (2014) 7813–7837.
[19] J.R. Rostrupnielsen, J.H.B. Hansen, J. Catal. 144 (1993) 38–49.
[20] L. Yue, F. Qi, F.S. Maria, Appl. Catal. B: Environ. 27 (2000) 179–191.
[21] F. Rahmani, M. Haghighi, P. Estifaee, Microporous Mesoporous Mater. 185 (2014) 213–223.
[22] K. Ray, S. Sengupta, G. Deo, Fuel Process. Technol. 156 (2017) 195–203.
[23] S.A. Theofanidis, V.V. Galvita, H. Poelman, G.B. Marin, ACS Catal. 5 (2015) 3028–3039.
[24] N. Lohitharn, J. Games Goodwin Jr, J. Catal. 257 (2008) 142–151.
[25] J. Dufour, C. Martos, A. Ruiz, F.J. Ayuela, Int. J. Hydrog. Energy 38 (2013) 7647–7653.
[26] N.M. Popova, R.-K. Salakhova, K. Dosumov, S.A. Tungatarova, A.S. Sass, Z.T. Zheksenbaeva, L.V. Komashko, V.P. Grigor'eva, A.A. Shapovalov, Kinet. Catal. 50 (2009) 567–576.
[27] Q. Liu, Z. Zhong, F. Gu, X. Wang, X. Lu, H. Li, G. Xu, F. Su, J. Catal. 337 (2016) 221–232.
[28] L. Pastor-Pérez, F. Baibars, E. Le Sache, H.A. García, S. Gu, T.R. Reina, J. CO_2 Util. 21 (2017) 423–428.
[29] L. Pei-Pei, W.Z. Lang, K. Xia, L. Luan, X. Yan, Y.J. Guo, Appl. Catal. A: Gen. 522 (2016) 172–179.
[30] N.K.G. Rosales, J.L. Ayastuy, M.P.G. Marcos, M.A. G-Ortiz, Catal. Today 176 (1) (2011) 63–71.
[31] L. Pastor-Pérez, R. Buitrago-Sierra, A. Sepulveda-Escribano, Int. J. Hydrog. Energy 39 (2014) 17589–17599.
[32] L.-H. Wang, S.X. Zhang, Y. Liu, Rare Earth 26 (2008) 66–70.
[33] Z. Hou, O. Yokota, T. Tanaka, T. Yashima, Appl. Surf. Sci. 233 (2004) 58–68.
[34] T. Stroud, T. Smith, E. Le Saché, J.L. Santos, M.A. Centeno, H.A. Garcia, J.A. Odriozola, T.R. Reina, Appl. Catal. B: Env. 224 (2018) 125–135.
[35] J. Aluha, Y.F. Hu, N. Abatzoglou, J. Catal. 7 (2) (2017) 69.
[36] A.B. Gaspar, J.L.F. Brito, L.C. Dieguez, J. Mol. Catal. A: Chem. 203 (2003) 251–266.
[37] Q. Liu, Z.Y. Zhong, F.N. Gu, X.Y. Wang, X.P. Lu, H.F. Li, G.W. Xu, F.B. Su, J. Catal. 337 (2016) 221–232.
[38] M. Liang, W. Kang, K. Xie, Nat. Gas Chem. 18 (2009) 110–113.
[39] O.H. Laguna, F. Romero-Sarria, M.A. Centeno, J.A. Odriozola, J. Catal. 276 (2010) 360–370.
[40] J.P. Bortolozzi, T. Weiss, L.B. Gutierrez, M.A. Ulla, J. Energy Chem. 246 (2014) 343–352.
[41] R.M. Navarro, R.G. Lopez, A.A. Ismail, S.A.A. Sayari, J.L.G. Fierro, Catal. Today 242 (2015) 60–70.
[42] P. Dufresne, E. Payen, J. Grimblot, J.P. Bonnelle, J. Phys. Chem. 85 (1981) 2344.
[43] S.D. Senanayake, J.A. Rodriguez, D. Stacchiola, Appl. Catal. A: Gen. 329 (2007) 68–78.
[44] D.H. Kim, S.W. Han, H.S. Yoon, Y.D. Kim, J. Energy Chem. 23 (2015) 67–71.
[45] Q. Liu, J.J. Gao, M.J. Zhang, H.F. Li, F.N. Gu, G.W. Xu, Z.Y. Zhong, F.B. Su, RSC Adv. 4 (2014) 16094–16103.
[46] C.H. Bartholomew, Appl. Catal. A: Gen. 212 (2001) 17–60.